Molecular-dynamics study of liquid mercury in the density region between metal and nonmetal

Tomonari Sumi
Department of Applied Physics, Faculty of Engineering, Kyushu University, Fukuoka 812-8581, Japan

Eisaku Miyoshi
Institute for Molecular Science, Okazaki 444-8585, Japan

Kiyoshi Tanaka
Division of Chemistry, Graduate School of Science, Hokkaido University, Sapporo 060-0810, Japan
(Received 27 August 1998)

Molecular dynamics (MD) calculations of expanded liquid mercury in the density region between metal and nonmetal were made using the potential energy curve of dimeric mercury (Hg_2) determined from molecular orbital calculations. The density dependence of the thermal pressure coefficient and the internal pressure, which were observed experimentally in the density region that included the metal-nonmetal transition range, were qualitatively demonstrated with our MD calculations. The change of calculated pair distribution function and structure factor from a metallic to a nonmetallic state also explained qualitatively the change of experimental ones. The temperature dependence of the isochoric electrical conductivity was discussed using quantities obtained from the calculated pair distribution functions. It was shown that the increase of the isochoric electrical conductivity accompanying an increase in temperature, which was experimentally observed in the strong-scattering metallic region, can be realized through the increase of the density of states at the Fermi energy arising from the decrease of interatomic distance. [S0163-1829(99)06809-5]

I. INTRODUCTION

Liquid mercury is transformed from a metal to a nonmetal when its density decreases. Measurements of the optical gap[1] and the Knight shift[2] suggest that this metal-nonmetal (M-NM) transition occurs at a density of around $\rho_{MN}=9\ g/cm^3$. Recently Kresse and Hafner[3] performed an *ab initio* simulation of the M-NM transition in expanded fluid mercury. They pointed out that the M-NM transition is simply a band-crossing transition, which is the typical transition expected in any divalent metal, according to the Bloch-Wilson band model, and that both disorder-induced electronic localization and electronic correlation effects might be of less importance. At a density of less than ρ_{MN}, i.e., in the nonmetallic state, the relationship between the thermoelectric power, S, and the electrical conductivity, σ, is that of a thermal activation-type semiconducting regime[4] and the isochoric σ actually increases as the temperature increases, namely, $(\partial\sigma/\partial T)_v>0$.[5] However the isochoric σ also increases with the temperature at densities above ρ_{MN}, i.e., in the metallic state. In the weak-scattering region ($11.0\leqslant\rho\leqslant13.6\ g/cm^3$),[6] where Ziman's nearly-free electron theory is valid, the increase of isochoric σ is attributable to the lower first peak of the structure factor with the higher temperature.[7] On the other hand, in the strong-scattering region ($9.0\leqslant\rho\leqslant11.0\ g/cm^3$) Ziman's formula becomes unsatisfactory, because the mean free path of electrons is not large compared with the mean atomic distance,[6] so the relationship between the isochoric σ and the temperature has not been investigated. It is interesting to investigate the behavior of the isochoric σ from the perspective of atomic arrangement and electronic structure.

The liquid-vapor coexistence curves of cesium and rubidium are remarkably different from those of typical nonmetallic fluids in their extreme asymmetry with respect to critical density, and they violate the law of rectilinear diameter.[8] Goldstein and Ashcroft[9] suggested that the difference between the liquid-vapor coexistence curves of metallic and simple nonmetallic systems arises from thermodynamic-state dependent effective particle interactions. They also attributed the strong thermodynamic-state dependence of the ion-ion interactions in a metallic system to the change in the screening effects of the electron cloud. For a nonmetallic system, Pester *et al.*[10] showed that it is possible to incorporate the effects of three-body dispersion (Axilrod-Teller) forces into a thermodynamic-state dependent on the effective particle interactions. Thus, we can regard this thermodynamic-state dependence on the effective particle interactions as one of the effects of many-body interactions, compared with two-body interactions. It has been reported that considering the relativistic effects and treating the $5d$ electrons explicitly leads to a strong damping of the Friedel oscillations, which arise from the screening effect of the electron cloud, in the effective pair potential of Hg.[11] Thus, we can expect that the many-body effects of Hg are smaller than those of alkali metals.

A number of experimental studies have reported thermodynamic properties, such as the thermal pressure coefficient and the internal pressure, in the density region between metal and nonmetal states.[5,12–14] Yao and Endo[5] predicted that these might be connected to the qualitative change of interatomic interactions arising from the M-NM transition, and with the thermodynamic-state dependence of these interatomic interactions. Molecular dynamics (MD) calculations

TABLE I. Binding energy D_e (cm^{-1}), bond length R_e (Å), vibrational frequency ω_e (cm^{-1}), and anharmonicity $\omega_e\chi_e$ (cm^{-1}) for the Hg_2 $^1\Sigma_g^+$ ground state.

Method	D_e (cm^{-1})	R_e (Å)	ω_e (cm^{-1})	$\omega_e\chi_e$ (cm^{-1})
SDCI	238	4.35	12	0.18
SDCI(+Q)	339	4.14	14	0.20
CPA	393	4.06	15	0.25
CPA (scaling)[a]	393	3.63	17	0.31
Expt.[b]	380±15		19.9±0.5	0.26±0.03
Expt.[c]	350±20		19±2	0.25
Expt.[d]		3.63±0.04	18.5±0.5	0.27

[a]The interatomic distance r is scaled with a factor of $d=1.12$ (see text).
[b]See Ref. 19.
[c]See Ref. 20.
[d]See Ref. 21.

have not been made for the broad density region between metal and nonmetal, because it is difficult to treat these effects explicitly.

Very recently, we performed MD calculations for liquid mercury near the melting point, using the potential energy curve of dimeric mercury (Hg_2) obtained from molecular orbital (MO) calculations.[15] By taking the approach that the electrons are divided between the ion cores and the electron cloud, the screening effects of itinerant electrons are explicitly expressed as the effective interionic potential, which has Friedel oscillations. However, our approach does not consider the screening effects of itinerant electrons explicitly, and the pair potential curve used in our study included the electron correlation between two atoms. The melting temperature obtained by the calculations agrees well with the experimental value. The MD calculations reproduced a characteristic feature of liquid metal, cooperative motions corresponding to the collective short-wavelength excitation in the dynamic structure factor. On the other hand, MD calculations using a Lennard-Jones potential did not give the same feature. This result showed that pair-potential approximation using the potential energy curve of Hg_2 produces a reasonable approximation of the force field in liquid metal mercury and that the contribution to the force field arising from many-body interactions rather than from two-body interactions is not necessarily important for the cooperative motions. The pair potential approximation using the potential energy curve of Hg_2 is expected to be a good approximation for expanded liquid mercury. In this paper, we perform MD calculations for expanded liquid mercury in a wide density region between liquid metal and liquid nonmetal that includes the vicinity of the M-NM transition, using the potential energy curve of Hg_2.

The methods and results of MO calculations are presented in Sec. II. The spectroscopic constants obtained by MO calculations are compared with observed values. In Sec. III, the methods of MD calculations are presented and the properties estimated by MD calculations are summarized and discussed in comparison with the experimental data. Concluding remarks are given in Sec. IV.

II. MO CALCULATIONS OF Hg_2

To obtain the pair potential curve for mercury, MO calculations were performed for the ground state of Hg_2 using the quasirelativistic model potential,[16] where the $5p$, $5d$, and $6s$ electrons were treated explicitly. The contraction scheme of Gaussian-type functions (GTF's) to the basis set $(s/p/d/f)$ was (6111*/511*1*1*/4111*/1*1*), where 1* denotes an additional GTF. The exponents of the respective additional GTF's were 0.0211 for the *s*-type, 0.135, 0.037, and 0.0174 for the *p*-type, and 0.062 for the *d*-type, and 1.46 and 0.73 for the *f*-type. The ground state of Hg_2 is weakly bound by the van der Waals forces arising from a closed-shell $5p^65d^{10}6s^2$ electron configuration. The Hartree-Fock (HF) calculation does not give the bound state to the ground state of Hg_2. In order to consider the correlation between the $5d$ and $6s$ electrons, we determined the singly and doubly excited configuration interaction (SDCI), the Davidson correction for the SDCI (SDCI+Q), and the coupled-pair approximation (CPA), which was developed by one of us (K.T.) in collaboration with others[17] and includes many-electron-excitation effects. The HF, SDCI, SDCI(+Q) and CPA calculations were performed using the ALCHEMY2 (Ref. 18) software package.

The results of the MO calculations for the ground $^1\Sigma_g^+$ state are summarized in Table I. In the SDCI calculation, the binding energy D_e is small and the bond length R_e is long compared with the experimental values.[19–21] When the many-electron-excitation effect is incorporated, D_e increases and R_e decreases. In the CPA calculations, D_e agrees with

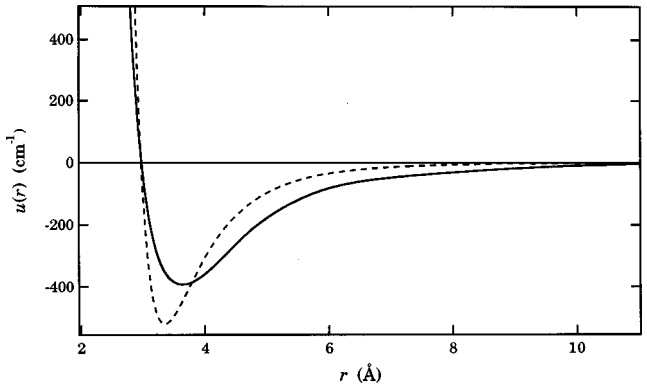

FIG. 1. Pair potentials. Modified CPA potential energy curve, $u_{CPA}(r)$, and a (12-6) Lennard-Jones potential, $u_{LJ}(r)$, derived from viscosity data (Ref. 22). Solid curve: $u_{CPA}(r)$. Dashed curve: $u_{LJ}(r)$.

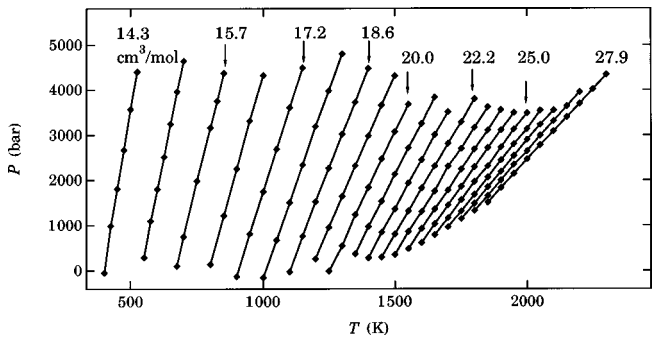

FIG. 2. Isochores for liquid mercury on the P-T plane. The densities are 14.3, 15.0, 15.7, 16.4, 17.2, 17.9, 18.6, 19.3, 20.0, 20.7, 21.4, 22.2, 22.9, 23.6, 24.3, 25.0, 25.7, 26.4, 27.2, and 27.9 cm^3/mol.

the experimental value extremely well, while R_e is 0.4 Å longer than the experimental value. The other constants obtained by CPA agree well with the experimental values.

III. MD CALCULATIONS OF LIQUID Hg

We performed MD calculations for expanded liquid mercury from the metallic to nonmetallic states by using the potential energy curve given by the CPA. The pair potential used in the MD calculations, $u_{\mathrm{CPA}}(r)$, was modified from the CPA potential energy curve, $\phi_{\mathrm{CPA}}(r)$, by using the equation $u_{\mathrm{CPA}}(r)=\phi_{\mathrm{CPA}}(rd)$. Here d is a scaling parameter. We chose $d=1.12$ $(=4.06/3.63)$, so that the modified pair potential reproduced the exact equilibrium distance for Hg_2. As seen in Table I, the other spectroscopic constants are in excellent agreement with the experimental values. Therefore the $u_{\mathrm{CPA}}(r)$ reproduces the accurate potential energy curve of Hg_2 ground state, so that we can examine whether or not the pair potential approximation with the potential energy curve of Hg_2 gives reasonable force field for liquid mercury by using $u_{\mathrm{CPA}}(r)$. The $u_{\mathrm{CPA}}(r)$ and a (12-6) Lennard-Jones (LJ) potential, $u_{\mathrm{LJ}}(r)$, with parameters for liquid mercury derived from viscosity data,[22] which was used to perform MD calculations near the melting points,[15] were shown in Fig. 1. The slopes of the repulsive part of $u_{\mathrm{CPA}}(r)$ are looser than that of $u_{\mathrm{LJ}}(r)$. The potential wells around equilibrium in $u_{\mathrm{CPA}}(r)$ is broader than that in $u_{\mathrm{LJ}}(r)$. The long-range attractive parts of $u_{\mathrm{CPA}}(r)$ are kept large compared with that of $u_{\mathrm{LJ}}(r)$.

The MD calculations were performed using a Verlet algorithm with $N=864$ particles in a canonical ensemble with an interval of $\Delta t=0.007$ ps. We calculated the isochores between 7.2 and 14.0 g/cm^3 for liquid mercury on the pressure (P) and temperature (T) plane. The physical quantities were determined from the statistical averages over 30 000 intervals, after the motion equations were integrated over at least 70 000 intervals.

The isochores on the P-T plane are shown in Fig. 2. The slope of an isochore decreases as the volume increases. The calculated data for the equation-of-state are expressed by the following form of the isochore equation: $P=\gamma_v T-P_0$, in which the thermal pressure coefficient, $\gamma_v=(\partial P/\partial T)_v$, and the internal pressure, $P_0=(\partial E/\partial V)_T$, where E is internal energy, depend mainly on the volume. Figures 3(a) and 3(b) show γ_v vs V and P_0 vs V curves, respectively. As seen in Fig. 3(a), the value of γ_v for a high density is larger than for a low density. The γ_v vs V curve is a continuous line and the value of $|d\gamma_v/dV|$ changes consecutively. The value of $|d\gamma_v/dV|$ in the high-density-liquid-metal region is obviously larger than that in the low-density-liquid-semiconductor region. This behavior of the γ_v vs V curve has been observed experimentally[5,12–14] and the MD calculations agree well with the observed data qualitatively. As seen in Fig. 3(b), the value of P_0 increases as the volume decreases in the density region ($\rho \leqslant 12$ g/cm^3). This behavior in the P_0 vs V curve obtained by the MD calculations agree well with the observed data[5,12–14] qualitatively. The calculated P_0 vs V curve has a maximum and then the P_0 decreases as the volume decreases. This behavior is comparable with the experimental data observed by Postill *et al.*[14] and is general for liquid. If many-body interactions are essential to describing the volume dependence in force field of

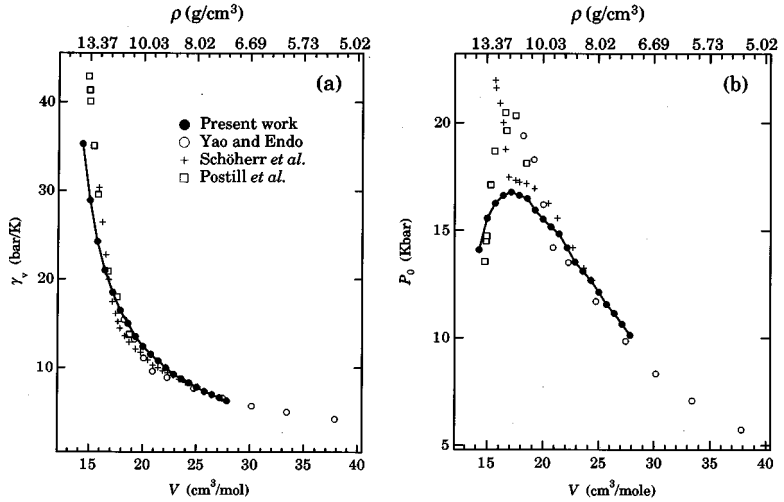

FIG. 3. (a) The thermal pressure coefficient γ_v for liquid mercury as a function of the molar volume. (b) The internal pressure P_0 for liquid mercury as a function of the molar volume. The solid circles are the result of MD calculations; the open circles are the data of Yao and Endo (Ref. 5); the crosses are the data of Schönherr *et al.* (Ref. 12); the squares are the data of Postill *et al.* (Ref. 14).

liquid mercury, then the behavior of γ_v vs V and P_0 vs V curves cannot be reproduced by our approach. However, the observed volume variations of γ_v and P_0 between the metallic and nonmetallic states can be demonstrated qualitatively by the pair-potential approximation using the potential curve of Hg_2. Therefore, the result shows that the change of force field between the metallic and nonmetallic regions can be reproduced by this approximation, and that many-body forces are not necessarily important for the volume dependence of γ_v and P_0. This observation indicates that the thermodynamic-state dependence of interatomic interactions, which corresponds to the density dependence in the canonical ensemble, is not essential to describe qualitatively the volume dependence of γ_v and P_0. From quantitative point of view, the both γ_v vs V and P_0 vs V curves estimated by the MD calculations in the high-density metallic region ($11 \leqslant \rho \leqslant 14\,\mathrm{g/cm^3}$) seem to deviate from the observed values slightly. These results suggest that the pair potential approximation using the potential energy curve of Hg_2 qualitatively reproduces the volume variation of force field, however, many-body effects may be important to discuss these properties quantitatively in high-density metallic region.

Tamura and Hosokawa[23] made x-ray diffraction measurements for expanded liquid mercury, including the M-NM transition range along the liquid-vapor coexistence curve. They pointed out that the expansion of liquid mercury in the metallic region ($11 \leqslant \rho \leqslant 14\,\mathrm{g/cm^3}$) is accompanied not by a uniform increase in the interatomic distance, r_1, but by a decrease of the coordination number, N_1. As the density decreases further, the relative rate of the decrease in N_1 becomes smaller and r_1 then starts to increase.[23] We calculated the pair distribution function, $g_{\mathrm{MD}}(r)$, and the structure factor, $S_{\mathrm{MD}}(k)$, in the density region between 7.2 and 14.0 g/cm^3. The $g_{\mathrm{MD}}(r)$ at three thermodynamic states: the metallic state (1273 K, 10.98 g/cm^3), the state near the M-NM transition (1673 K, 9.25 g/cm^3), and nonmetallic state (1803 K, 6.6 g/cm^3), are shown in Figs. 4(a), 4(b), and 4(c), respectively, compared with the corresponding pair distribution functions, $g_{\mathrm{x\,ray}}(r)$, obtained from the Fourier transformation of structure factors determined by x-ray diffraction measurement.[23] The r_1 becomes longer as the volume and temperature increases. The behavior is qualitatively consistent with those seen in $g_{\mathrm{x\,ray}}(r)$. However some details in the shape of $g_{\mathrm{MD}}(r)$ is different from the corresponding $g_{\mathrm{x\,ray}}(r)$. In the $g_{\mathrm{x\,ray}}(r)$, there is a broad band inside the first peak and the first peak has a shoulder in its outside. These differences can be attributed to the difference between $g_{\mathrm{x\,ray}}(r)$ and $g_{\mathrm{MD}}(r)$: as x-ray diffraction originates from x-ray beams scattered by the electrons, the $g_{\mathrm{x\,ray}}(r)$ is associated with the correlation between the electrons, while the $g_{\mathrm{MD}}(r)$ shows the distribution of atomic nuclei. Figures 5(a), 5(b), and 5(c) show the $S_{\mathrm{MD}}(k)$ at three thermodynamic states corresponding to Figs. 4(a), 4(b), and 4(c), respectively, compared with the $S_{\mathrm{x\,ray}}(k)$. The $S_{\mathrm{MD}}(k)$'s agree well with the $S_{\mathrm{x\,ray}}(k)$'s at all thermodynamic states. The first peak shifts to the small-k side and the width of first peak is broadening with increasing volume and temperature. It should be noted that there appears a minimum in the small-k region below 1 Å^{-1} for both $S_{\mathrm{MD}}(k)$ and $S_{\mathrm{x\,ray}}(k)$ at the low-density-nonmetallic state [Fig. 5(c)], which indicates significant decrease of long-range order.

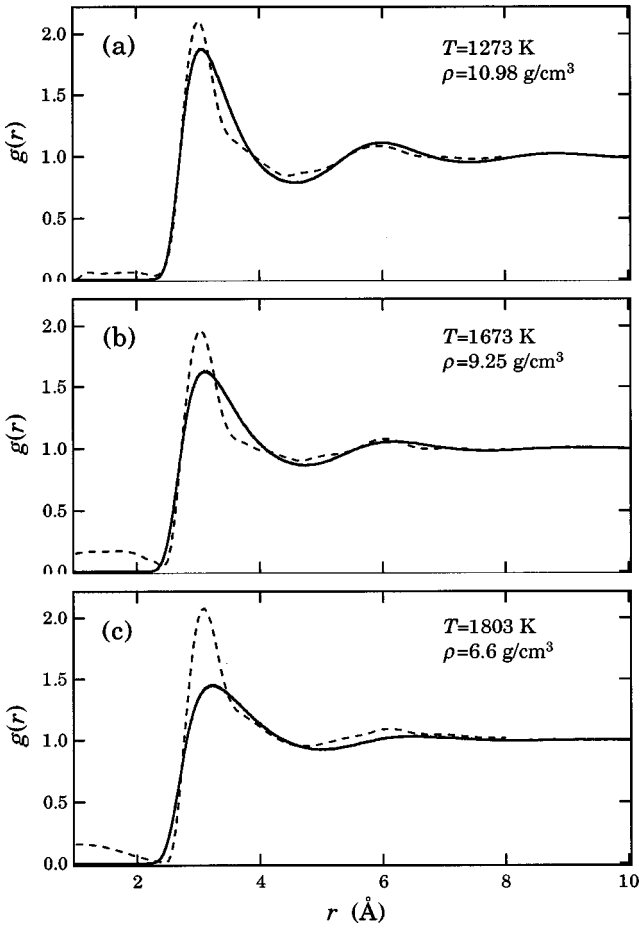

FIG. 4. The pair distribution function for three thermodynamic states. (a) (1273 K, 10.98 g/cm^3). (b) (1673 K, 9.25 g/cm^3). (c) (1803 K, 6.6 g/cm^3). Solid lines: MD calculation; dashed lines: x-ray diffraction data (Ref. 23).

The variation of r_1 and N_1 with temperature for fixed volumes is shown in Figs. 6(a) and 6(b), respectively. As seen in Figs. 6(a) and 6(b), r_1 increases and N_1 decreases with volume at a fixed temperature. It is notable that r_1 decreases with increasing temperatures at a fixed volume. Higher temperature, in other words, increasing kinetic energies of Hg atoms lead to strong collision between atoms, then r_1 becomes short at a fixed volume. When the density decreases from 14 to 11 g/cm^3, r_1 increases from 3.06 to 3.09 Å and N_1 decreases from 7.3 to 5.3. On the other hand, when the density decreases from 11 to 8 g/cm^3, r_1 increases from 3.09 to 3.18 Å and N_1 decreases from 5.3 to 3.9. Thus, in the high-density region ($11 \leqslant \rho \leqslant 14\,\mathrm{g/cm^3}$), the density dependence of r_1 is relatively small and the decrease in r_1 with an increase in temperature is large, and the density and temperature dependence of N_1 are also both relatively large. In the low-density region ($8 \leqslant \rho \leqslant 11\,\mathrm{g/cm^3}$), r_1 becomes very density dependent, but becomes much less temperature dependent, and N_1 is much less dependent on density and temperature. These results explain the density dependence of the structure of liquid mercury seen in the experimental data.[23]

We tried to interpret the thermodynamic-state dependence of the electrical conductivity σ in the metallic strong-scattering region ($9.0 \leqslant \rho \leqslant 11.0\,\mathrm{g/cm^3}$) from the perspective

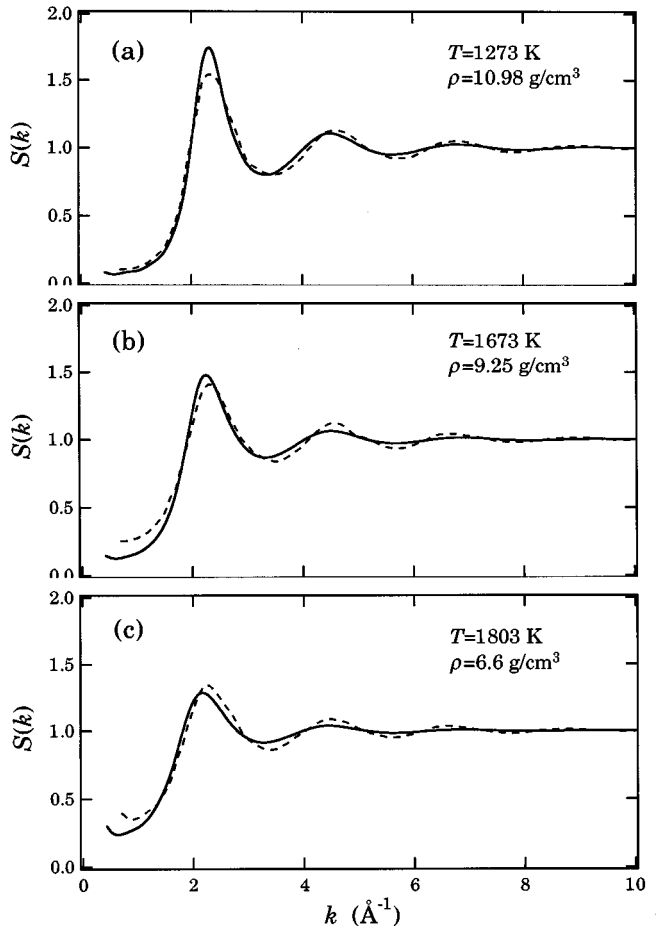

FIG. 5. The structure factor $S(k)$ for three thermodynamic states. (a) (1273 K, 10.98 g/cm^3). (b) (1673 K, 9.25 g/cm^3). (c) (1803 K, 6.6 g/cm^3). Solid lines: MD calculation; dashed lines: x-ray diffraction data (Ref. 23).

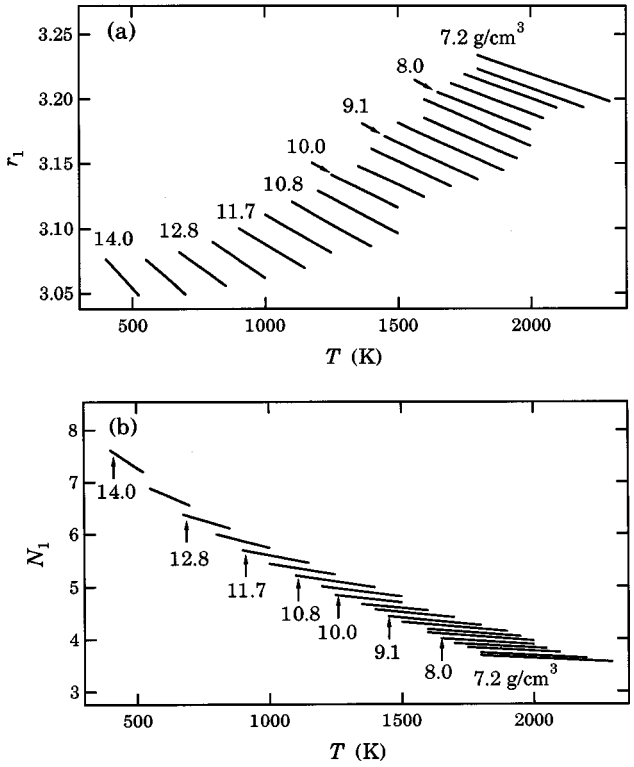

FIG. 6. (a) Isochores of the nearest-neighbor distance r_1 for liquid mercury. (b) Isochores of the coordination number N_1 for liquid mercury.

of the change in atomic arrangements obtained by the MD calculations. As mentioned at the beginning of this paper, the temperature dependence of isochoric σ in this strong-scattering region has been found in a number of experimental studies: the isochoric σ increases as the temperature increases, i.e., $(\partial\sigma/\partial T)_v > 0$. The M-NM transition of expanded liquid mercury is simply a band-crossing transition, which is arising from the vanishing of overlap between the tails of $6s$ and $6p$ band. In the strong-scattering region, the overlap between $6s$ and $6p$ band is small, then the density of states at the Fermi energy, $N(E_F)$, is also small. According to tight-binding approximation, the bandwidth B is generally given by $B=2N_1I$,[24] where I is the overlap energy integral and increases exponentially with decreasing interatomic distance. As seen in Fig. 5, r_1 and N_1 decrease with higher temperature at a fixed volume. Generally these exponential increases of I with decreasing r_1 overcome the decreases of N_1. Thus B increases with higher temperatures under a fixed volume, so that the increasing overlap between the tails of $6s$ and $6p$ band leads to the increasing of density of states at the Fermi energy. Therefore, the isochoric electrical conductivity, which is proportional to the square of the density of states at Fermi energy, increases as temperature increases.

IV. CONCLUSIONS

In this study, we performed SDCI, SDCI(+Q), and CPA calculations for the ground $^1\Sigma_g^+$ state of Hg_2 incorporating the $5d$ and $6s$ electron correlations and major relativistic effects. The many-electron-excitation effect produces spectroscopic constants close to the experimental values. Therefore the electron correlation effect is very important for describing the interaction between mercury atoms.

MD calculations for expanded liquid mercury were performed using the potential energy curve of Hg_2, in the regions including the M-NM transition range. The volume dependence of the thermal pressure coefficient, γ_v, and the internal pressure, P_0, estimated by the MD calculations agree well with experimental results. Therefore, many-body interactions or the qualitative change in the form of interatomic interactions arising from density dependence are not necessarily essential to explain the behavior of the γ_v vs V and the P_0 vs V curves. The variation of calculated pair distribution function between metallic and nonmetallic state qualitatively demonstrates the variation of experimental ones. We discussed that the thermodynamic-state dependence of the electrical conductivity σ in the strong-scattering region from the viewpoint of the change in atomic arrangements obtained by the MD calculations. The increase of the isochoric electrical conductivity accompanying an increase in temperature can be realized through the increase of the density of states at the Fermi energy arising from the decrease of interatomic distance. In the preceding paper,[15] we reported that the MD calculations near the melting point using the potential curve of Hg_2 reproduce the cooperative motion corresponding to the collective short-wavelength excita-

tions in the dynamic structure factor. These results suggest that pair-potential approximation using the potential curve of the dimeric molecule gives a good qualitative description of the metallic interatomic force for liquid mercury, and MD calculations using this approximation demonstrate the characteristic change of force fields between liquid metal and liquid semiconductor. However, the both γ_v vs V and P_0 vs V curves estimated by the MD calculations seem to deviate from the observed values slightly in the high-density metallic region. These differences between the observed and calculated values may be attributed to the lack of the many-body effects.

It has been pointed out[10] that the relative importance of three-body interactions compared with two-body interactions in the liquid-vapor critical range for mercury is larger than for other van der Waals molecules. The boiling point determined by the present MD calculations is much higher than the observed value. This higher temperature should be corrected by considering three-body effects, such as the Axilrod-Teller interaction,[25] because the three-body dispersion forces are repulsive while the two-body dispersion force is a long-range attractive force. It is interesting to determine the liquid-vapor coexistence curve with pair-potential approximation using the potential energy curve of Hg_2 and to investigate the contribution of three-body effects to the liquid-vapor transition phenomena, especially in liquid-vapor critical range.

ACKNOWLEDGMENTS

The authors would like to thank Dr. Megumu Yoshimine for allowing us to use the ALCHEMY2 software package. A part of the calculations in this study were performed on the IBM RS/6000 SP2 cluster in the Computer Center of Institute for Molecular Science. This research was partly supported by a Grant-in-Aid for Scientific Research from the Ministry of Education, Science and Culture of Japan.

[1] H. Uchtmann and F. Hensel, Phys. Lett. **53A**, 239 (1975).
[2] W. W. Warren, Jr. and F. Hensel, Phys. Rev. B **26**, 5980 (1982).
[3] G. Kresse and J. Hafner, Phys. Rev. B **55**, 7539 (1997).
[4] M. Yao and H. Endo, J. Phys. Soc. Jpn. **51**, 1504 (1982).
[5] M. Yao and H. Endo, J. Phys. Soc. Jpn. **51**, 966 (1982); M. Yao, K. Takehana, and H. Endo, J. Non-Cryst. Solids **205-207**, 270 (1996).
[6] N. F. Mott, Philos. Mag. **13**, 989 (1966); Adv. Phys. **16**, 49 (1967); Philos. Mag. **17**, 1259 (1968); **19**, 835 (1969).
[7] J. M. Ziman, Philos. Mag. **6**, 1013 (1961); T. E. Febar and J. M. Ziman, *ibid.* **11**, 153 (1965).
[8] S. Jüngst, B. Knuth, and F. Hensel, Phys. Rev. Lett. **55**, 2160 (1985).
[9] R. E. Goldstein and N. W. Ashcroft, Phys. Rev. Lett. **55**, 2164 (1985).
[10] M. W. Pestak, R. E. Goldstein, M. H. W. Chan, J. R. de Bruyn, D. A. Balzarini, and N. W. Ashcroft, Phys. Rev. B **36**, 599 (1987).
[11] W. Jank and J. Hafner, Phys. Rev. B **42**, 6926 (1990).
[12] G. Schönherr, R. W. Schmutzler, and F. Hensel, Philos. Mag. B **40**, 411 (1979).
[13] F. E. Neale, N. E. Cusack, and R. D. Johnson, J. Phys. F **9**, 113 (1979).
[14] D. R. Postill, R. G. Ross, and N. E. Cusack, Philos. Mag. **18**, 519 (1968).
[15] T. Sumi, E. Miyoshi, Y. Sakai, and O. Matsuoka, Phys. Rev. B **57**, 914 (1998).
[16] Y. Sakai, E. Miyoshi, M. Klobukowski, and S. Huzinaga, J. Comput. Chem. **8**, 256 (1987).
[17] K. Tanaka, T. Sakai, and H. Terashima, Theor. Chim. Acta **76**, 213 (1989); T. Sakai and K. Tanaka, *ibid.* **85**, 451 (1993).
[18] B. H. Lengsfield III, J. Chem. Phys. **73**, 382 (1980); B. Liu and M. Yoshimine, *ibid.* **74**, 612 (1981); B. H. Lengsfield III and B. Liu, *ibid.* **75**, 478 (1981).
[19] J. Koperski, J. B. Atkinson, and L. Krause, Chem. Phys. Lett. **219**, 161 (1994).
[20] A. Zehnacker, M. C. Duval, C. Jouvet, C. Lardeux-Dedonder, D. Solgadi, B. Soep, and O. B. d'Azy, J. Chem. Phys. **86**, 6565 (1987).
[21] R. D. van Zee, S. C. Blankespoor, and T. S. Zwier, J. Chem. Phys. **88**, 4650 (1988).
[22] R. C. Reid, J. M. Prausnitz, and B. E. Poling, *The Properties of Gases and Liquids*, 4th ed. (McGraw-Hill, New York, 1987).
[23] K. Tamura and S. Hosokawa, Phys. Rev. B **58**, 9030 (1998); J. Phys.: Condens. Matter **6**, A241 (1994); J. Non-Cryst. Solids **156/158**, 646 (1993).
[24] N. F. Mott, *Metal-Insulator Transitions*, 2nd ed. (Taylor & Francis, London, 1990), Chap. 1.
[25] B. M. Axilrod and E. Teller, J. Chem. Phys. **11**, 299 (1943).